HHS Public Access

Author manuscript

Nat Commun. Author manuscript; available in PMC 2012 December 10.

Published in final edited form as:

Nat Commun. ; 3: 614. doi:10.1038/ncomms1629.

Programmable Multivalent Display of Receptor Ligands using Peptide Nucleic Acid Nanoscaffolds

Ethan A. Englund[1,*], **Deyun Wang**[1,*], **Hidetsugu Fujigaki**[2,*], **Hiroyasu Sakai**[2], **Christopher M. Micklitsch**[1], **Rodolfo Ghirlando**[3], **Gema Martin-Manso**[4], **Michael L. Pendrak**[4], **David D. Roberts**[4], **Stewart R. Durell**[2], and **Daniel H. Appella**[1]

[1]Laboratory of Bioorganic Chemistry, NIDDK, NIH

[2]Laboratory of Cell Biology, CCR, NCI, NIH

[3]Laboratory of Molecular Biology, NIDDK, NIH

[4]Laboratory of Pathology, CCR, NCI, NIH

Abstract

Multivalent effects dictate the binding affinity of multiple ligands on one molecular entity to receptors. Integrins are receptors that mediate cell attachment through multivalent binding to peptide sequences within the extracellular matrix, and overexpression promotes the metastasis of some cancers. Multivalent display of integrin antagonists enhances their efficacy, but current scaffolds have limited ranges and precision for the display of ligands. Here we present an approach to study multivalent effects across wide ranges of ligand number, density, and three-dimensional arrangement. Using L-lysine γ-substituted peptide nucleic acids, the multivalent effects of an integrin antagonist were examined over a range of 1 to 45 ligands. The optimal construct improves the inhibitory activity of the antagonist by two orders of magnitude against the binding of melanoma cells to the extracellular matrix in both *in vitro* and *in vivo* models.

Introduction

Multivalency describes the simultaneous binding of multiple ligands on one molecular entity to multiple receptors on another entity. Multivalent interactions require precise spatial orientation of ligands and receptors at the nanometer scale, and dysregulation can be responsible for progression of diseases, such as the metastasis of cancer. Integrins are a class

Correspondence and requests for materials should be addressed to D.H.A. (appellad@niddk.nih.gov).

*These authors contributed equally to this work.

Supplementary Information (please link to an online version)

Author Contributions:

E.A.E. and D.W. performed the syntheses, characterizations, and assemblies of all PNAs and associated complexes, H.F. and H.S. performed cell-based assays and *in vivo* studies, C.M.M. developed the conjugation procedure to attach ligands to PNAs, R.G. performed the analytical ultracentrifugation, G.M-M., M.L.P., and D.D.R. performed the echistatin competition assays and provided and maintained all the cell lines, S.R.D. performed all the computer modeling. The manuscript was written by E.A.E., S.R.D., and D.H.A. The initial ideas were conceived by D.H.A.

The authors declare no competing financial interests.

of membrane-associated proteins that mediate cell attachment and motility through multivalent binding, and a subset of these proteins (such as $\alpha_v\beta_3$) bind to the Arg-Gly-Asp (RGD) tripeptide sequence motif of extracellular matrix proteins[1,2]. The expression of integrin $\alpha_v\beta_3$ is increased on certain tumor cells[3], and antagonists, such as Cilengitide[4], have shown efficacy in clinical trials for metastatic melanoma and glioblastoma[5,6]. Multivalent display of integrin antagonists has been used to enhance their efficacy[2,7–12], but current scaffolds for the display of ligands have physical limitations that constrict the range and precision of multivalent arrangements that can be explored[13]. Herein we present an approach to make ligand-conjugated scaffolds that supports comprehensive screening for multivalent effects across wide ranges of ligand number, density, and three-dimensional arrangement.

Historically, the development of synthetic scaffolds at the nanometer scale for the multivalent display of ligands can be broken down into two strategies: step-by-step and shotgun. The step-by-step approach involves sequentially attaching individual, ligand-containing units via covalent bonds (Fig. 1a)[14]. In this case, the number of desired ligands dictates the number of required synthetic steps. While this method yields more precision in terms of ligand number and relative orientation, in most cases it is logistically impractical for valencies greater than ~10 ligands. In contrast, the shotgun approach involves the single-step coupling (or polymerization) of multiple ligands to a preexisting scaffold, such as a dendrimer, gold nanoparticle, polymer, or protein (Fig. 1b)[15]. While this can lead to high valencies, it is at the expense of knowing the exact number and/or relative orientation of the ligands. Furthermore, shotgun methods often result in an unknown, complex mixture of species that may further complicate analysis of biological activity. Translation of nanotechnology to medical therapies relies on nanometer-scale scaffolds in which bioactive ligands can be displayed with a high degree of precision to facilitate optimization of biological activity[16,17]. Ideally, the synthesis of such scaffolds would be facile and flexible, allowing for the rapid study of bioactivity over a wide range of different ligand valencies and densities.

In this Article, we present a scaffold and general strategy that overcomes the limitations of previous approaches (Fig 1c). The core of the scaffold is a hybrid of peptide nucleic acid (PNA) and single-stranded DNA (ssDNA). PNA molecules are oligomers with a peptide-like backbone, typically formed from aminoethylglycine (*aeg*), with nucleic acid bases as sidechains (Fig. 2a). This allows for stable, complementary binding to DNA or RNA[18,19]. Substituting one or more of the regular *aeg*PNA residues in the synthesis with a monomer that contains an attachment point allows cyclic-RGD-containing ligands, which are antagonists of $\alpha_v\beta_3$ integrins, to be placed anywhere along the PNA. For this step, we used L-lysine γ-substituted peptide nucleic acid (^{L}Kγ-PNA), whose lysine sidechain is available for conjugation and does not interfere with nucleic acid binding[20–22]. Finally, using nucleic acid-driven assembly of ligand-conjugated ^{L}Kγ-PNA oligomers and ssDNA containing varying numbers of repeating complementary sequences, we can rapidly form libraries of multivalent molecules with precise numbers and densities of ligands (Figs. 1c, 2b, 2c). Specific for the current report, we designed ^{L}Kγ-PNA to control the assembly of a derivative of Cilengitide into fifty-two individual multivalent constructs over a range of 1 to 45 ligands

that spanned different ligand arrangements and densities. The biological activities of each construct were examined and the optimal construct improves the inhibitory activity of the drug by two orders of magnitude against the binding of melanoma cells to the extracellular matrix in both *in vitro* cell-based and *in vivo* mouse models. We anticipate that scaffolds constructed from ^{L}Kγ-PNA will greatly impact studies on multivalent display because the scaffold can be prepared with many different biological ligands and varied ranges of ligand valency, density, and arrangement can be explored with high levels of precision for each construct.

Results

Multivalent Library

To demonstrate the utility of our strategy, we developed a library of multivalent PNA-DNA complexes to block the attachment of metastatic melanoma cells to the extracellular matrix. For the ligand, we used a cyclic-RGD analog, cycloArg-Gly-Asp-dPhe-Lys (c(RGDfK))[4], with a short polyethylene glycol (PEG) linker to competitively bind to the $\alpha_v\beta_3$ integrins on the cell's surface. The c(RGDfK) ligand had previously been examined with valencies between 2 to 16 using step-by-step approaches[3], and with average valencies between 13 and 52 with shotgun approaches[3,23]. In contrast, we designed a 52-member library that systematically varies the position, density, and number of ligands from 1 to 45 (Fig. 3a). To modulate the positions and density of ligands we synthesized four different 12-residue PNA oligomers: A) single ligand at the N-terminus, B) single ligand at the center, C) two ligands, and D) three ligands (B, C, and D have the ligand attached via an ^{L}Kγ-PNA sidechain, Supplementary Fig. S1). Each one of these PNA's was annealed with one of thirteen different ssDNA's with repeats of the complementary sequence from 1 to 15 (Supplementary Table S1). To identify each construct, we refer to a complex consisting of a ssDNA with *x* adjacent sequence repeats complementary to a PNA with sidechains as DNA:PNA-Y_X, where *x* is an integer from 1 to 15 and *Y* is a letter (A–D) representing one of the four different PNA's.

Cell-based screen for multivalent effects

The first test was a screen to determine the ability of each member of the library to inhibit C32 human melanoma cells from attachment to a vitronectin–coated surface (Fig. 3a)[24]. The expression and specific function of $\alpha_v\beta_3$ integrin for attachment has been previously established for this cell line[24]. The experiments were controlled by the use of unattached c(RGDfK) molecules alone, which allowed results from different days to be normalized. Each experiment was performed at six different concentrations of each DNA:PNA-Y_X inhibitor, and each concentration was repeated in triplicate, to determine IC_{50} values. The results are shown in Fig. 3b, Supplementary Fig. S2 and Supplementary Table S2. Since the inhibitory activities of PNA's A and B were similar, the two sets of results were combined into one series (A/B) in Fig. 3b. When increasing the number of ligands per PNA from one to two to three (PNA A/B to C to D), the activity continually increases when each PNA is complexed to complementary DNA with one consensus sequence (IC_{50} values are 477, 169, and 67 nM, respectively, for DNA:PNA-Y_1). This suggests that DNA:PNA-D_1 can bind three $\alpha_v\beta_3$ integrin receptors simultaneously. We confirmed that such a multivalent

interaction is sterically possible by developing an atomic-scale computer model of the complex with an arbitrary arrangement of the receptors in a cell membrane (Fig. 4). Increases in activities also occur as the number of consensus sequence repeats in the ssDNA increases. The results show that the activity plateaus around 5–11 repeats of the consensus sequence in the ssDNA (depending on which PNA is used), with maximal improvement of inhibitory activity approximately two orders of magnitude vs. the c(RGDfK) control. The effect of increasing the distance between adjacent PNAs was examined with PNA-B and ssDNA consisting of complimentary consensus sequences that were separated by additional thymines (Supplementary Fig. S3). While some improvement in activity was observed using DNA with two and three consensus sequences, the effect was not significant with longer DNAs. We interpret these data to indicate that proper spacing between ligands is important for interaction with multiple integrin receptors, but at higher valencies there is a local concentration effect that simultaneously contributes. These results are consistent with other multivalent assemblies of RGD[7,25–28]. Examination of the full multivalent landscape (Fig. 3b) allowed selection of the construct DNA:PNA-D_5 for further binding and *in vivo* studies. This construct displays 15 cyclo-RGD ligands and was selected because it has the most potent inhibitory activity with the shortest ssDNA sequence.

Competition assay

Quantitative measurements of the dissociation constant for DNA:PNA-D_5 binding to $\alpha_v\beta_3$ were conducted using competitive displacement experiments against radiolabled ^{125}I-echistatin binding to C32 melanoma cells. Echistatin is a 49 residue snake venom peptide with a single RGD motif that binds strongly to $\alpha_v\beta_3$ (K_d = 0.3 nM) and other integrins[29]. The displacement curves for individual tests of DNA:PNA-D_5 and the c(RGDfK) control are shown in Figure 5a. Similar to the previous results (Fig. 3b), the multivalent DNA:PNA-D_5 has a dissociation constant two orders of magnitude lower than monovalent c(RGDfK) (K_d values of 0.16 nM vs. 62.9 nM, respectively). The displacement of ^{125}I-echistatin further confirms that the RGD ligands of DNA:PNA-D_5 bind to the receptor sites on the integrins.

In vivo activity

Next, we investigated the *in vivo* activity of DNA:PNA-D_5 using a mouse melanoma cell line (B16F10). *In vitro* analysis using the aforementioned cell-adhesion assay showed B16F10 cells responded to the DNA:PNA constructs in a manner consistent with C32 cells (Supplementary Table S3). B16F10 cells injected into the tail vein rapidly metastasize and form tumors in the lungs[30]. This mouse model was selected over subcutaneous models because the mechanism of Cilengitide is known to inhibit metastasis under these conditions and provides a direct readout of any improvement due to multivalent effects[31,32]. Previous studies have demonstrated that lung colonization by B16F10 cells in this experimental metastasis model can be significantly reduced through the use of integrin receptor ligands[31,32]. Compared to the control group receiving only B16F10 cells, mice dosed with 2 mgs of unconjugated c(RGDfK) (2.4 μmol) displayed about a 30% reduction in tumor colonies upon sacrifice (Figs. 5b, 5c) after 14 days. However, mice that were treated with 0.1 mgs of DNA:PNA-D_5 ($1.7\bullet10^{-3}$ μmol of complex, or $2.6\bullet10^{-2}$ μmol c(RGDfK), which amounts to 1% of the number of c(RGDfK) molecules relative to the control sample) showed an average reduction of approximately 50%. Thus, the efficacy of each c(RGDfK)

unit appended to the DNA:PNA-D_5 scaffold increased by about two orders of magnitude over c(RGDfK) alone. Mice treated with ssDNA or PNA alone, or with DNA:PNA complexes without attached c(RGDfK) ligands, did not exhibit any reduction in lung colonization.

Stoichiometry and Stability

Finally, analytical ultracentrifugation was used to verify the stoichiometry and stability of the constructs. Although the DNA:PNA duplexes used in these studies are thermodynamically stable, as evidenced by annealing experiments, higher order complexes are harder to confirm, and cases of partial or nonspecific binding are difficult to identify. Accordingly, we tested DNA:PNA-B_5, which should have 5 PNA-B molecules binding to 5 contiguous complementary sequence repeats in the ssDNA and is the same length as DNA:PNA-D_5. Sedimentation experiments revealed its presence at 3.21S (Fig. 5d, $s_{20,w}$ = 3.31S), and a hybrid local continuous/global discrete analysis yielded an average molecular mass of 43.9 ± 1.1 kDa (42.41875 kDa predicted). Furthermore, the well-defined peak for the complex across the multiple concentrations suggests that the DNA:PNA-B_5 construct is not in equilibrium with remaining free PNA. Although PNA oligomers can aggregate in solution reducing the binding efficiency to complementary sequences, there was no evidence of unbound ssDNA.

Discussion

Complexes of DNA with ligand-modified ^{L}Kγ-PNA should be a general strategy to overcome the limitations of traditional nanometer-sized scaffolds and accurately control the presentation of biological ligands. Notably, the ability to rapidly produce a systematically-varied library over a broad range of valencies and geometries allows for a clear determination of the optimal configuration. In this case, it was relatively simple to identify the multivalent DNA:PNA-D_5 construct with 15 c(RGDfK) ligands to inhibit $\alpha_v\beta_3$ integrin binding with activity two orders of magnitude greater than c(RGDfK) alone in both *in vitro* and *in vivo* assays. At the present time it is not clear why improvement of multivalent activity levels off around 15 ligands, but we hypothesize that steric crowding of integrin receptors prevents higher-valency constructs from contributing additional benefits to activity. Based on recent clinical data with Cilengetide[5,6], its likely the DNA:PNA-D_5 construct alone does not have therapeutic value; however, in combination with imaging or chemotherapeutic agents it could be beneficial for tumor targeting[3,4].

Comparing with other multivalent RGD constructs in the literature that explore similar valency levels, our optimized scaffold demonstrates remarkable activity. For example, a Regioselectively Addressable Functionalised Template (RAFT) based on a cyclic decapeptide scaffold was made via step-by-step synthesis with 16 RGD ligands, but it did not show improved activity compared to the same scaffold with a valency of 2 ligands[12]. Another study explored a shotgun approach where RGD was conjugated to an antibody to achieve an average valency of 13 ligands per protein and an improvement in activity of each RGD by about 32 times compared to the monovalent ligand[33]. Each of these studies, however, examined only 5 different multivalent assemblies, likely due to the labor

associated with preparing the scaffolds and conjugating the ligand. In our approach, we were able to screen 52 different multivalent assemblies over a valency range of 1 to 45 ligands to find an optimal one that improved the potency of each RGD ligand by about 2 orders of magnitude. We believe this strategy, in addition to a recently published γ-Cys-version[22], could greatly aid the exploration of multivalent assemblies especially if incorporated with other strategies to manipulate the three-dimensional architecture of DNA[34].

Methods

Synthesis of PNA

Commercial-grade reagents and solvents were used without further purification except as indicated. The resin (MBHA, 100–200 mesh, 1% DVB, 0.3 mmol/g, Advanced Chemtech, Louisville, KY, USA) was prepared by swelling in DCM and downloading the resin with Boc-protected mPEG to 0.1 mmol/g capacity. Boc-protected *aeg*PNA monomers were purchased from PolyOrg, Inc. (Leominster, MA, USA). PNA oligomer synthesis was carried out on a 5 μmol scale on an Applied BioSystems 433A Automated Peptide Synthesizer. Resin was swelled with DCM for 90 minutes before synthesis. ^{L}Kγ-PNA Monomer was synthesized according to published procedures[35]. Activated ^{L}Kγ-PNA monomer was allowed 180 minutes to couple. An additional treatment of TFA deprotection solution was also used to deblock ^{L}Kγ-PNA residues. The lysine sidechains of ^{L}Kγ-PNA monomers (Fmoc) were orthogonally deprotected with 20% piperidine in DMF. When multiple ^{L}Kγ-PNA residues were present in the PNA oligomer (PNA-C and PNA-D, Fig. 3a), the primary amines on the sidechains were deprotected and coupled to mPEG residues in tandem. Purification of PNA oligomers were carried out using a X-Bridge Prep. BEH 130 C18 5 μm (10 × 250 mm) column on an Agilent 1100 HPLC. In all cases, 0.05% aqueous trifluoroacetic acid and acetonitrile were used as solvents.

Preparation of Multivalent Constructs

A solution of ^{L}Kγ-PNA (1.5 μmol), 3,4-diethoxy-3-cyclobutene-1,2-dione (45 μmol, 30 equiv), triethylamine (90 μmol, 60 equiv), 500 μl of anhydrous DMSO and 250 μl of absolute ethanol was mixed for 3 hour. The solution was concentrated and the residue was washed with diethyl ether (3×1.0 ml), and dried under vacuum to get the squaric acid-conjugated PNA intermediate as a white solid. The above PNA intermediate was added to a solution of c(RGDfK(PEG-PEG) (30 μmol, 20 equiv, Peptides International, Louisville, KY, USA), triethylamine (45 μmol, 30 equiv) in 500 μl of anhydrous DMSO and 250 μl of absolute ethanol. After 18 hours of shaking, the solution was concentrated. The residue was purified by HPLC (19 × 150 mm Waters C8 reverse phase column, 12 ml/min flow rate, 0.1% aqueous trifluoroacetic acid and acetonitrile) to obtain the final product (57%~90% yield over two steps) as a white solid. Conjugates were characterized by mass spectrometry using an Agilent 1200 series quadrupole LC/MSD electrospray trap (Supplementary Table S4). To make PNA:DNA complexes, a 1x PBS buffer solution of 20 μM DNA (Supplementary Table S1, Integrated DNA Technologies, Inc. (USA)) was combined with the appropriate concentration of PNA conjugate depending on the repeat unit number on the DNA (UV quantification was performed using either a Nanodrop ND 1000, or an Agilent

8453 UV-Vis Spectrophotometer) at 25 °C. The solution was heated to 92 °C and held for 5 min, and then slowly cooled down to 25 °C over a period of 3 hours.

Cell culture and cell attachment assay

C32 and B16F10 cells were maintained in RPMI1640 medium supplemented with 10% FCS, 2 mM L-glutamine, and penicillin and streptomycin in an incubator at 37°C in a humidified atmosphere containing 5% CO_2. The cell attachment assay was carried out as previously described[36]. Collagen Type I was purchased from Advanced BioMatrix. Vitronectin, BSA, Bouin's solution, and Echistatin were purchased from Sigma. 96-well flat-bottom plates were purchased from NUNC. All other cell culture media and medium supplements were purchased from Gibco. Either collagen Type I or vitronectin diluted in Dulbecco's PBS (DPBS without Ca^{2+}, Mg^{2+}) was coated onto 96-well flat-bottom plates (NUNC) overnight at 4 °C. After aspiration of the buffer, nonspecific adherence to plastic was blocked by incubation with DPBS containing 1% BSA at room temperature for 30 min. Cells were harvested and washed in DPBS and resuspendend at 1×10^6 cells/ml in serum free RPMI1640 containing 0.1% BSA. Aliquots of cells (50 μl) were added to each well containing 50 μl of the indicated concentrations of c(RGDfV) or PNA construct diluted in serum free RPMI1640 containing 0.1% BSA. The plate was incubated at 37 °C for 45 min to allow the cells attach to the plate. After the incubation, medium was discarded and nonadherent cells were removed by washing the plate with DPBS (with Ca^{2+}, Mg^{2+}). The number of adherent cells was quantified using the previously described colorimetric hexosaminidase assay[37].

Molecular Modeling

Atomic-scale, computer models were developed with the QUANTA Modeling Environment software program (Accelrys, Inc.; 10188 Telesis Ct.; Suite 100; San Diego, CA 92121; www.accelrys.com). The models were illustrated with the UCSF Chimera package from the Resource for Biocomputing, Visualization, and Informatics at the University of California, San Francisco (supported by NIH P41 RR001081)[38]. The extended $\alpha_v\beta_3$ integrin model was developed from the crystal structure of a 'bent' conformation as described by Xiong et al. (PDB accession code: 1JV2)[39]. The c(RGDfV) moiety was positioned analogous to the cyclic-RGD analog in the subsequent$\alpha_v\beta_3$ integrin crystal structure: PDB accession code: 1L5G[40]. The DNA:PNA-Y_x construct models were developed from PDB accession code: 1PDT[41].

^{125}I-Echistatin Competition Assay

Echistatin iodination was carried out by the Chloramine T (N-chloro tosylamide) method[42]. This procedure typically yielded a specific activity of 17.5 μCi/μg. Competitive binding assays were carried out using a fixed amount of radioactive tracer added to varying concentrations of unlabeled competitor in the presence of 10^5 C32 cells per tube. Triplicate samples were incubated at 25 °C on a rocking platform. Bound and free ligands were separated by centrifugation through a Nyosol M25 oil cushion. Non-specific binding was assessed using 20-fold excess unlabeled echistatin as a competitor. The success of a PNA binding experiment was assessed by a comparison with a competitive displacement

experiment using c(RGDfK) peptide carried out at the same time. The data was non-linearly fit to the 2-ligand, single receptor, heterologous displacement model using the LIGAND software program[43]. For this, the echistatin association constant for binding to $\alpha_v\beta_3$ integrin was fixed at the published value of 3.33×10^9 M[42].

Animals and tumor metastasis assay

8–10 week old female C57BL/6Cr mice were obtained from Charles River. All animal protocols used in this study were approved by the National Cancer Institute Animal Safety and Use Committee. All *in vivo* studies were conducted using DNA with phosphorothioate overhangs on each side in order to retard any degradation *in vivo*[44]. B16F10 cells were detached from culture flask and resuspended to 5×10^6/ml. Cyclo-RGD or PNA complex were then mixed with cells and 0.2 ml aliquots containing 2 mg of RGD, 100 μg of PNA complex, or PBS and single cell suspensions of 5×10^5 cells were injected slowly into the lateral tail vein. Fourteen days later the animals were euthanized with CO_2 and their lungs were excised and fixed in Bouin's solution. The number of surface melanoma colonies was counted visually.

Sedimentation studies on the DNA:PNA-B_5 complex

Sedimentation velocity experiments were performed on the DNA:PNA-B_5 complex prepared with a slight excess of PNA-B. Initial c(*s*) analyses were consistent with the presence of both a DNA:PNA-B_5 complex at 3.20 S (uncorrected) and excess monomeric and dimeric PNA-B. The well-defined peak for the complex observed at all loading concentrations, together with a constant loading ratio of free PNA-B to complex, would suggest that these species are not in equilibrium with each other. Consequently, the appropriate c(*s*) analysis should allow for an estimate of the complex molecular mass. A two dimensional c(*s*, f/f_o) model was initially implemented[45]. At all concentrations studied, the projected c(*s*,*) distribution shows the presence of the complex at 3.21 ± 0.02 S, corresponding to an $s_{20,w}$ of 3.31 ± 0.02 S, as well as monomeric and dimeric PNA-*B* (Fig. 3a). Based on the best-fit average f/f_o of 1.95 for the complex, a value consistent with the expected asymmetry of the double stranded complex, an average molecular mass of 46.0 kDa is estimated for the complex. Though this value is slightly larger than that expected for the 5:1 complex which has a calculated mass of 42.41875 kDa, it supports the 5:1 stoichiometry for the complex. Data were analyzed on terms of a hybrid local continuous/global discrete model in SEDPHAT. In this model, the excess PNA-*B* is accounted for in terms of a continuous c(s) distribution, whereas the complex is modeled as a discrete species with single values for *s*, M and f/f_o. Experiments carried out at three loading concentrations yield identical results, within the error of the method, returning an average $s_{20,w}$ of 3.31 ± 0.004 S and an average molecular mass of 43.9 ± 1.1 kDa supporting a 5:1 stoichiometry for the DNA:PNA-B_5 complex (n = 1.03 ± 0.03). Sedimentation experiments on the 60 base ssDNA show that this is a monodisperse monomer with a sedimentation coefficient of 2.771 ± 0.007 S and a partial specific volume of 0.541 cm^3g^{-1}. Similar experiments on a complementary 12 base PNA show that this self-associates to form a dimer with a K_d of 0.85 ± 0.2 μM. Additional sedimentation velocity controls can be found in the Supplementary Methods.

Supplementary Material

Refer to Web version on PubMed Central for supplementary material.

Acknowledgments

This work was supported by the Intramural Programs of the NIDDK and NCI at NIH. We thank Gail McMullen for assistance with mice, Sergio Coelho for assistance with photography, and George Lieman and Lisa Jenkins for helpful comments. We dedicate this paper to the memory of Dr. Ryan Monfeli.

References

1. Campbell ID, Humphries JM. Integrin structure, activation, and interactions. Cold Spring Harb Perspect Biol. 2011; 3:a004994. [PubMed: 21421922]
2. Nemeth JA, et al. Aplha-v Integrins as Therapeutic Targets in Oncology. Cancer Invest. 2007; 25:632–646. [PubMed: 18027153]
3. Auzzas L, et al. Targeting αvβ3 integrin: design and applications of mono-and multifunctional RGD-based peptides and semipeptides. Curr Med Chem. 2010; 17:1255–1299. [PubMed: 20166941]
4. Mas-Moruno C, Rechenmacher F, Kessler H. Cliengitide: The First Anti-Angiogenic Small Molecule Drug Candidate. Design, Synthesis and Clinical Evaluation. Anticancer Agents Med Chem. 2010; 10:753–768. [PubMed: 21269250]
5. Stupp R, et al. Phase I/IIa Study of Cilengitide and Temozolomide With Concomitant Radiotherapy Followed by Cilengitide and Temozolomide Maintenance Therapy in Patients With Newly Diagnosed Glioblastoma. J Clin Oncol. 2010; 28:2712–2718. [PubMed: 20439646]
6. Bradley DA, et al. Cilengitide (EMD 121974, NSC 707544) in asymptomatic metastatic castration resistant prostate cancer patients: a randomized phase II trial by the prostate cancer clinical trials consortium. Invest New Drugs. 201010.1007/s10637-010-9420-9428
7. Thumshirn G, Hersel U, Goodman SL, Kessler H. Multimeric Cyclic RGD Peptides as Potential Tools for Tumor Targeting: Solid-Phase Peptide Synthesis and Chemoselective Oxime Ligation. Chem Eur J. 2003; 9:2717–2725. [PubMed: 12772286]
8. Lee BW, et al. Strongly Binding Cell-Adhesive Polypeptides of Programmable Valencies. Angew Chem Int Ed Engl. 2010; 49:1971–1975. [PubMed: 20148425]
9. Jin ZH, et al. Effect of Multimerization of a Linear Arg-Gly-Asp Peptide on Integrin Binding Affinity and Specificity. Biol Pharm Bull. 2010; 33:370–378. [PubMed: 20190395]
10. Galibert M, et al. Application of click-click chemistry to the synthesis of new multivalent RGD conjugates. Org Biomol Chem. 2010; 8:5133–5138. [PubMed: 20835451]
11. Temming K, Schiffelers RM, Molema G, Kok RJ. RGD-based strategies for selective delivery of therapeutics and imaging agents to the tumour vasculature. Drug Resist Updat. 2005; 8:381–402. [PubMed: 16309948]
12. Garanger E, Boturyn D, Coll JL, Favrot MC, Dumy P. Multivalent RGD synthetic peptides as potent $\alpha_V\beta_3$ integrin ligands. Org Biomol Chem. 2006; 4:1958–1965. [PubMed: 16688341]
13. Wang J, Tian S, Petros RA, Napier ME, Desimone JM. The complex role of multivalency in namoparticles targeting the transferring receptor for cancer therapies. J Am Chem Soc. 2010; 132:11306–11313. [PubMed: 20698697]
14. Kiessling LL, Gestwicki JE, Strong LE. Synthetic multivalent ligands in the exploration of cell-surface interactions. Curr Opin Chem Biol. 2000; 4:696–703. [PubMed: 11102876]
15. Subbiah R, Veerapandian M, Yun KS. Nanoparticles: functionalization and multifunctional applications in biomedical sciences. Curr Med Chem. 2010; 17:4559–4577. [PubMed: 21062250]
16. Mammen M, Choi SK, Whitesides GM. Polyvalent Interactions in Biological Systems: Implications for Design and Use of Multivalent Ligands and Inhibitors. Angew Chem Int Ed. 1998; 37:2754–2794.
17. Giljohann DA, et al. Gold Nanoparticles for Biology and Medicine. Angew Chem Int Ed Engl. 2010; 49:3280–3294. [PubMed: 20401880]

18. Egholm M, et al. PNA hybridizes to complementary oligonucleotides obeying the Watson-Crick hydrogen-bonding rules. Nature. 1993; 365:566–568. [PubMed: 7692304]
19. Nielsen PE. Peptide Nucleic Acids (PNA) in Chemical Biology and Drug Discovery. Chem Biodivers. 2010; 7:786–804. [PubMed: 20397216]
20. Englund EA, Appella DH. γ-Substituted Peptide Nucleic Acids Constructed from L-Lysine are a Versatile Scaffold for Multifunctional Display. Angew Chem Int Ed Engl. 2007; 46:1414–1418. [PubMed: 17133633]
21. Gorska K, Huang KT, Chaloin O, Winssinger N. DNA-templated homo- and heterodimerization of peptide nucleic acid encoded oligosaccharides that mimic the carbohydrate epitope of HIV. Angew Chem Int Ed Engl. 2009; 48:7695–7700. [PubMed: 19774579]
22. Scheibe C, Bujotzek A, Dernedde J, Weber M, Seitz O. DNA-programmed spatial screening of carbohydrate-lectin interactions. Chem Sci. 2011; 2:770–775.
23. Montet X, Funovics M, Montet-Abou K, Weissleder R, Josephson L. Multivalent Effects of RGD Peptides Obtained by Nanoparticle Display. J Med Chem. 2006; 49:6087–6093. [PubMed: 17004722]
24. Sipes JM, Krutzsch HC, Lawler J, Roberts DD. Cooperation between thrombospondin-1 type 1 repeat peptides and $\alpha_v\beta_3$ integrin ligands to promote melanoma cell spreading and focal adhesion kinase phosphorylation. J Biol Chem. 1999; 274:22755–22762. [PubMed: 10428859]
25. Cavalcanti-Adam EA, et al. Cell spreading and focal adhesion dynamics are regulated by spacing of integrin ligands. Biophys J. 2007; 92:2964–2974. [PubMed: 17277192]
26. Arnold M, et al. Induction of cell polarization and migration by a gradient of nanoscale variations in adhesive ligand spacing. Nano Lett. 2008; 8:2063–2069. [PubMed: 18558788]
27. Chakraborty S, et al. Evaluation of ^{111}In-labeled cyclic RGD peptides: tetrameric not tetravalent. Bioconjug Chem. 2010; 21:969–978. [PubMed: 20387808]
28. Kubas H, et al. Multivalent cyclic RGD ligands: influence of linker lengths on receptor binding. Nucl Med Biol. 2010; 37:885–891. [PubMed: 21055618]
29. Marcinkiewicz C, Vijay-Kumar S, McLane MA, Niewiarowski S. Significance of RGD Loop and C-Terminal Domain of Echistatin for Recognition ofαIIbβ3 andαvβ3 Integrins and Expression of Ligand-Induced Binding Site. Blood. 1997; 90:1565–1575. [PubMed: 9269775]
30. Fidler IJ. Biological behavior of malignant melanoma cells correlated to their survival in vivo. Cancer Res. 1975; 35:218–224. [PubMed: 1109790]
31. Oliva IB, et al. Effect of RGD-disintegrins on melanoma cell growth and metastasis: involvement of the actin cytoskeleton, FAK and c-Fos. Toxicon. 2007; 50:1053–1063. [PubMed: 17854854]
32. Ramos OH, et al. A novel αvβ3-blocking disintegrin containing the RGD motive, DisBa-01, inhibits bFGF-induced angiogenesis and melanoma metastasis. Clin Exp Metastasis. 2008; 25:53–64. [PubMed: 17952617]
33. Kok RJ, et al. Preparation and functional evaluation of RGD-modified proteins as $\alpha_v\beta_3$ integrin directed therapeutics. Bioconjug Chem. 2002; 13:128–135. [PubMed: 11792188]
34. Douglas SM, et al. Self-assembly of DNA into nanoscale three-dimensional shapes. Nature. 2009; 459:414–418. [PubMed: 19458720]
35. Englund EA, Appella DH. Synthesis of γ-substituted peptide nucleic acids: A new place to attach fluorophores without affecting DNA binding. Org Lett. 2005; 7:3465–3467. [PubMed: 16048318]
36. Kuznetsova SA, et al. TSG-6 binds via its CUB_C domain to the cell-binding domain of fibronectin and increases fibronectin matrix assembly. Matrix Biol. 2008; 27:201–210. [PubMed: 18042364]
37. Landegren U. Measurement of cell numbers by means of the endogenous enzyme hexosaminidase – applications to detection of lymphokines and cell-surface antigens. J Immunol Methods. 1984; 67:379–388. [PubMed: 6200537]
38. Pettersen EF, et al. UCSF chimera – A visualization system for exploratory research and analysis. J Comput Chem. 2004; 25:1605–1621. [PubMed: 15264254]
39. Xiong JP, et al. Crystal structure of the extracellular segment of integrin alpha V beta 3. Science. 2001; 294:339–345. [PubMed: 11546839]

40. Xiong JP, et al. Crystal structure of the extracellular segment of integrin αVβ3 in complex with an Arg-Gly-Asp ligand. Science. 2002; 296:151–155. [PubMed: 11884718]
41. Eriksson M, Nielsen PE. Solution structure of a peptide nucleic acid DNA duplex. Nature Struct Biol. 1996; 3:410–413. [PubMed: 8612069]
42. Kumar CC, et al. Chloramine T-induced structural and biochemical changes in echistatin. FEBS Lett. 1998; 429:239–248. [PubMed: 9662425]
43. Munson PJ, Rodbard D. Ligand – a versatile computerized approach for characterization of ligand-binding systems. Anal Biochem. 1980; 107:220–239. [PubMed: 6254391]
44. Pandolfi D, Rauzi F, Capobianco ML. Evaluation of different types of end-capping modifications on the stability of oligonucleotides toward 3′-and 5′-exonucleases. Nucleosides Nucleotides. 1999; 18:2051–2069. [PubMed: 10549151]
45. Brown PH, Schuck P. Macromolecular size-and-shape distributions by sedimentation velocity analytical ultracentrifugation. Biophys J. 2006; 90:4651–4661. [PubMed: 16565040]

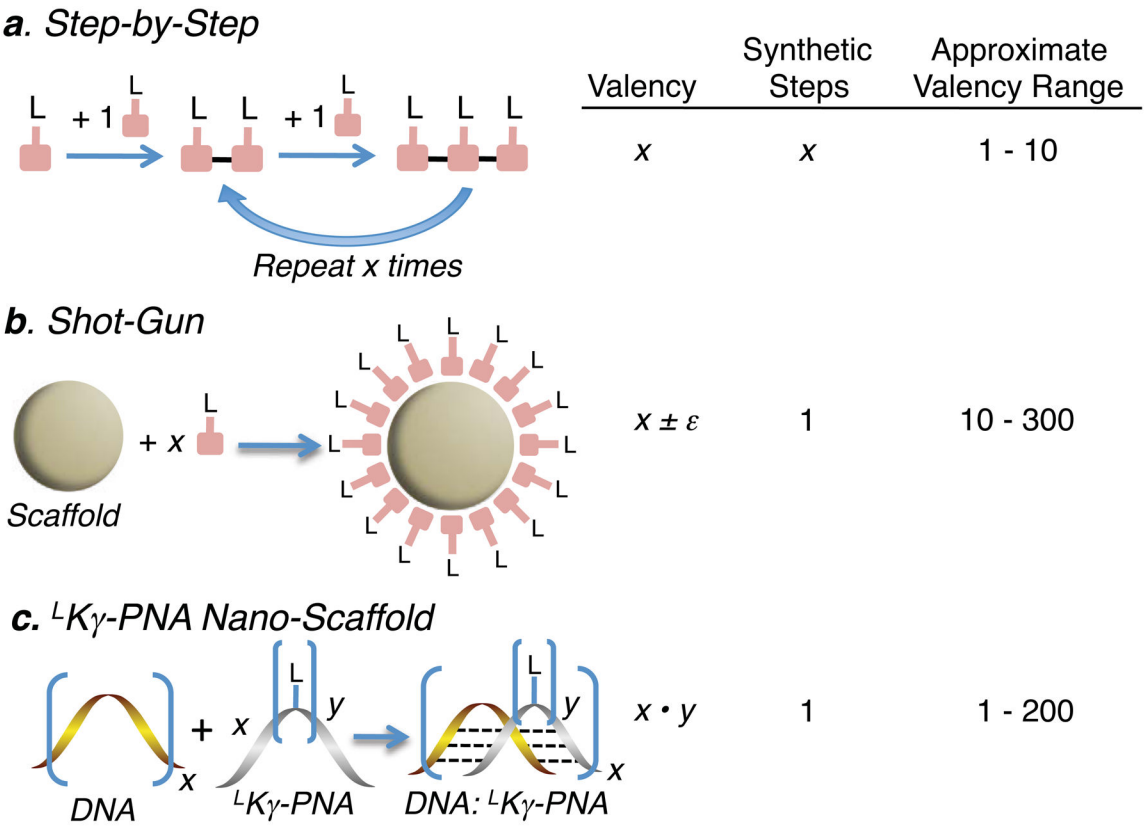

Valency	Synthetic Steps	Approximate Valency Range
x	*x*	1 - 10
x ± ε	1	10 - 300
x • *y*	1	1 - 200

Figure 1.

Strategies to construct multivalent assemblies. *a*. Step-by-Step syntheses afford an accurate valency but are limited to low numbers of ligands. *b*. Shotgun methods provide high valencies but an error (ε) is always associated with the number of ligands. *c*. Scaffolds made using L-lysine γ-substituted peptide nucleic acid (^{L}Kγ-PNA) and nucleic acid (NA) allow access to multivalent assemblies with both high valencies and accurate ligand number. Valency of an ^{L}Kγ-PNA-NA assembly is the product of the number of complementary binding sites incorporated into the NA (*x*) and the number of ligands displayed from each PNA oligomer (*y*).

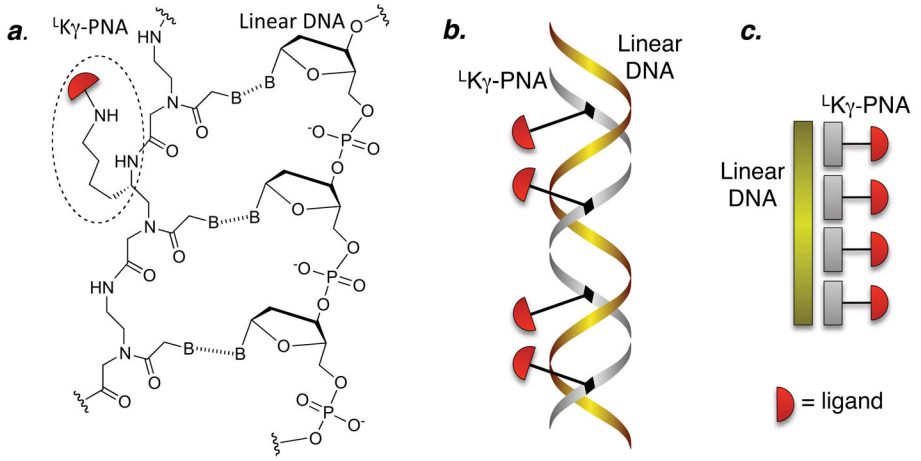

Figure 2.

Chemical and cartoon representations of ^{L}Kγ-PNA assembled onto DNA. *a.* Chemical structure of ^{L}Kγ-PNA bound to DNA. *b.* and *c.* Ribbon and cartoon diagrams of four ^{L}Kγ-PNAs (each bearing one ligand) bound to a linear DNA.

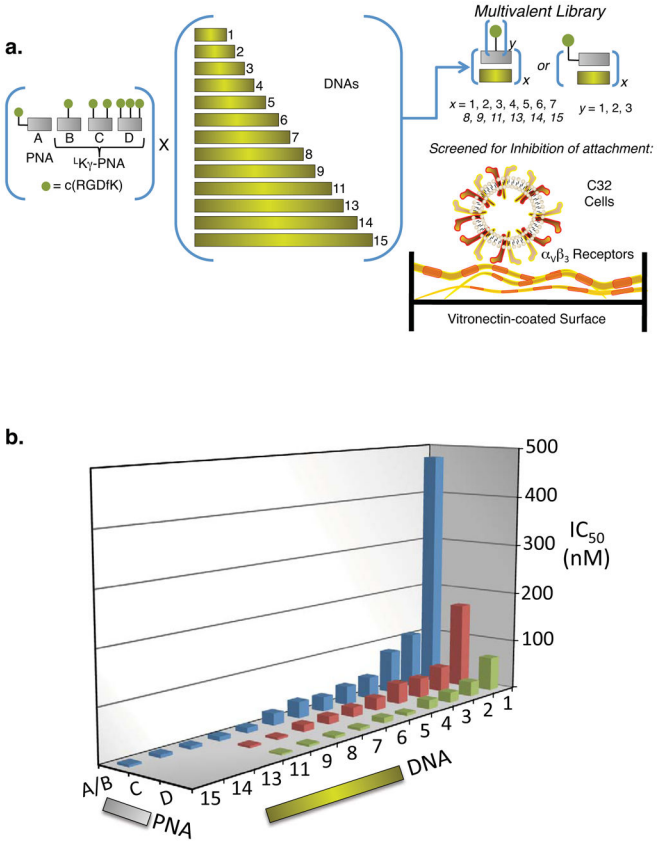

Figure 3.

Construction and screening of the DNA:PNA-Y_x multivalent library. *a.* Generation of the multivalent library by complexing each PNA in the first box with every DNA in the second box. PNA-A is an *aeg*PNA oligomer with a c(RGDfK) bound to the N terminus. PNA-B, PNA-C and PNA-D have 1, 2 or 3 c(RGDfK) units respectively, conjugated via γ-sidechains of internal ^{L}Kγ-PNA residues. DNA is numbered according to how many complementary sequences each contains and represents the number of PNAs that would be complexed. Inhibition of C32 cell adhesion to vitronectin was examined with DNA:PNA complexes. *b.* Three-dimensional representations of IC_{50} data from the screen of the library (A/B represents results from either PNA A or B). Data for DNA:PNA-$C/D_{13–15}$ were not acquired because inhibitory activity was maximized at shorter lengths of ssDNA (see Supplementary Fig. S2 for error bars).

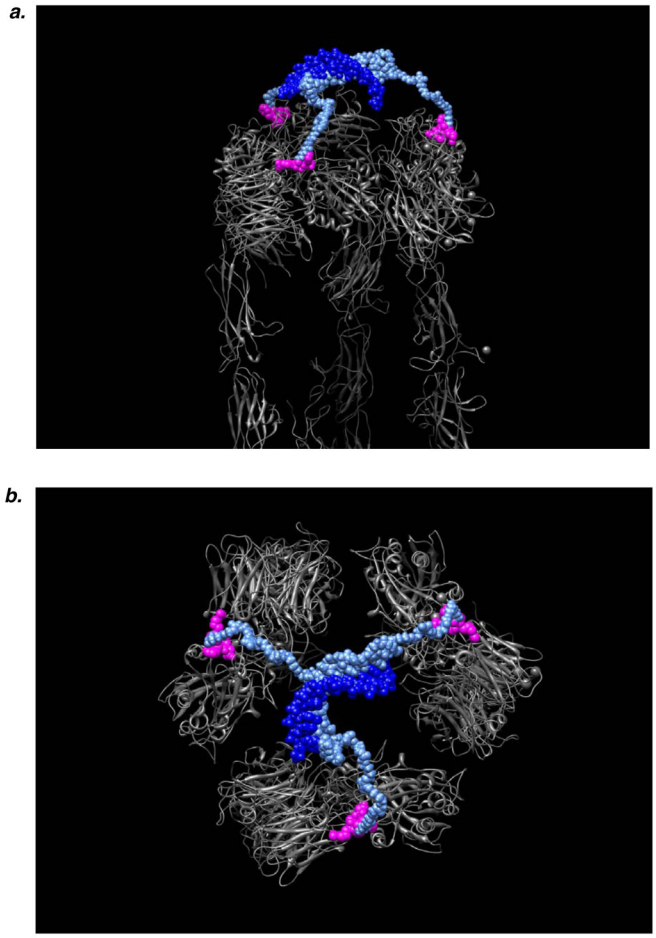

Figure 4.

Atomic-scale computational model of an ^{L}Kγ-PNA:DNA complex bound to $\alpha_V\beta_3$ integrin receptors. *a.* and b. The side and top views of a molecular model of DNA:PNA-D_1 bound to a cluster of three integrins (colored in pewter). The DNA template is dark blue, the ^{L}Kγ-PNA (including all bases and linkers are sky blue), and c(RGDfK) residues are fuchsia.

a.

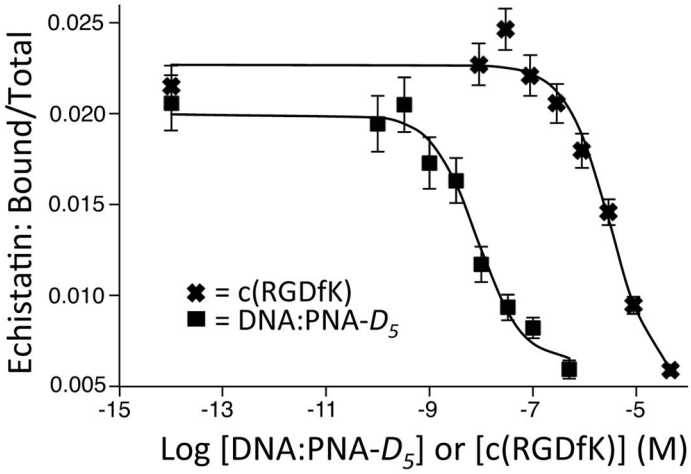

b.

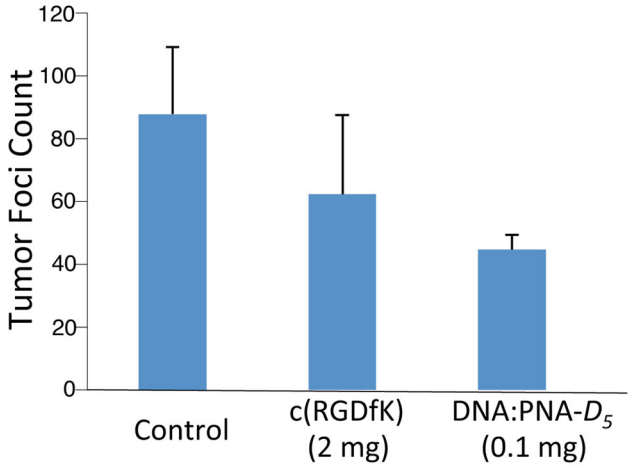

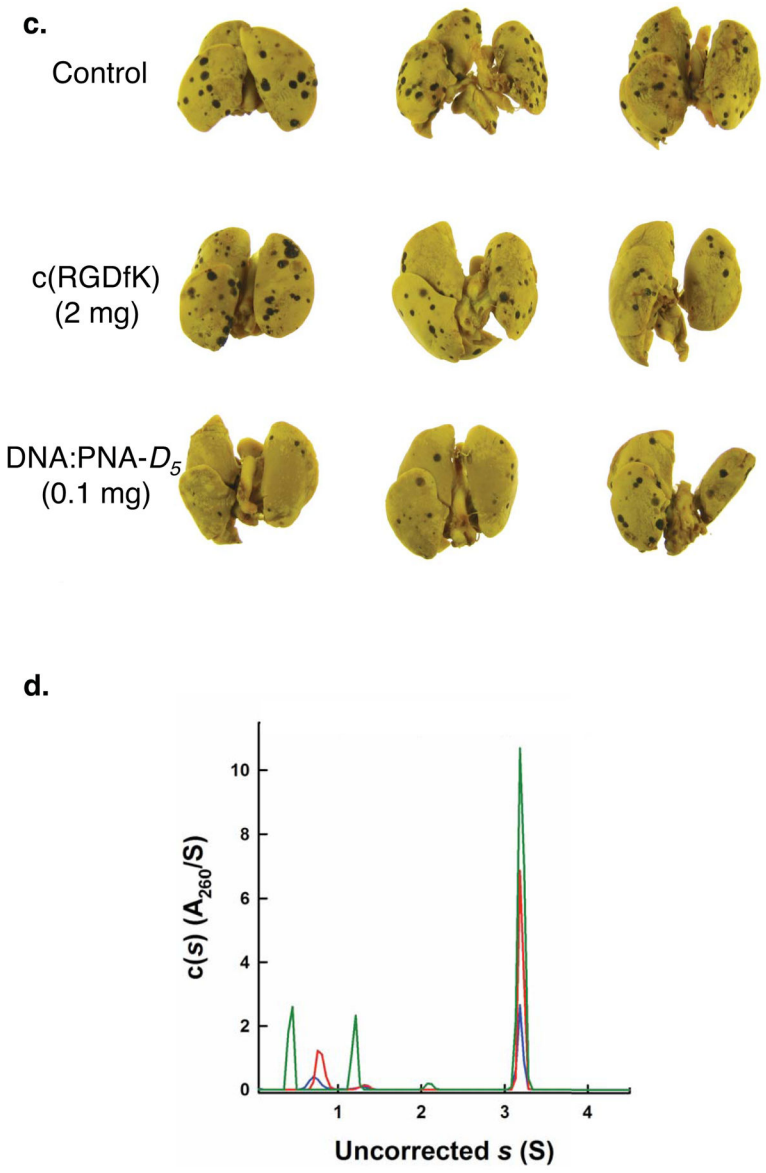

Figure 5.

in vivo activity and determination of stoichiometry for ^{L}Kγ-PNA:DNA complexes. *a.* Displacement of ^{125}I-Echistatin from integrin $\alpha_V\beta_3$ on C32 cells by c(RGDfK) and DNA:PNA-D_5. K_d c(RGDfK) = 6.3×10^{-8} M; K_d DNA:PNA-D_5= 1.6×1^{-10} M. Error bars represent two s.d. (n=3). *b.* The effect of DNA:PNA-D_5 on metastatic potential of B16F10 cells based on the tumor development in C57BL/6NCrmice. All mice were injected with 5×10^5 B16F10 cells. Error bars represent one s.d. (n=8 mice). *c.* Lungs of sacrificed mice after fixation with tumor lesions indicated by dark spots. The mice treated with DNA:PNA-D_5 had visibly fewer tumor colonies present after 14 days compared to the control or c(RGDfK) alone. Each row corresponds to three mice out of a group of eight. *d.* Absorbance c(s) distributions obtained from sedimentation velocity data collected at 50 krpm and 20.0

°C for DNA:PNA-B_5 at loading concentrations of 0.35 (blue), 0.78 (red) and 1.47 (green) A_{260}. The complex was prepared using a slight excess of PNA seen at ~1.0 S.